Dalton Transactions

Paper

Thermal stability of mesoscopic compounds of cetyl-trimethylammonium and Keggin metatungstates†

Received 00th January 20xx,
Accepted 00th January 20xx

DOI: 10.1039/x0xx00000x

www.rsc.org/dalton

A. C. Colusso,[a] M. B. Cortie[a], A. Dowd,[a] and A. McDonagh[a]

A hybrid surfactant/polyoxometalate compound was synthesized by combining isopolytungstate anions with the cationic surfactant cetyltrimethylammonium bromide (CTA-Br) to produce a hierarchical compound that we identify as $(CTA)_7[H_2W_{12}O_{40}]Cl.2H_2O$. At room temperature the compound consisted of hexagonally ordered sheets of Keggin ions, with an intervening gallery containing alkyl-chains of the organic cations. The synthesis was highly dependent on solution pH, reaction time and the order in which the reactants were added. We examined the effect of temperature on the stability of $(CTA)_7[H_2W_{12}O_{40}]Cl.2H_2O$ using thermal gravimetric analysis, differential scanning calorimetry, FT-IR spectroscopy and *in-situ* synchrotron X-ray diffraction, and found a step-wise conversion to monoclinic WO_x via a series of intermediates. Heating under nitrogen atmospheres accelerated transition events by ~100°C when compared to heating in air. During heating, the interplanar gallery at first expanded in a series of steps starting at 90°C as the CTA^+ amphiphiles changed orientation, before collapsing rapidly at 240°C, a temperature coinciding with the removal of about 40% of the organic material. Between 240 and 320°C, the material consisted of fragments of the Keggin ion cores, arranged in 2D hexagonally-packed sheets. At ~330°C, the Keggin ions were completely destroyed and replaced by bulk $W_{17}O_{47}$ which, upon further heating, transformed to bulk WO_2 or WO_3 depending on the environment.

Introduction

Tungsten oxides form a diverse and technologically versatile group of materials. The system is very complex: not only does WO_3 itself have at least seven different polymorphs, but there are also a range of mixed valence compounds with the generic formula W_nO_{3n-1}.[1-3] In addition, there are several polyoxometalates (POMs) — discrete nanocluster anions constructed of W(VI) and oxygen.[4-6] POMs are usually comprised of W, Mo or V, and O, which form cyclic geometries resulting in macromolecular clusters.[7] There are many variations of such discrete entities, especially because of the transition metals' mixed-valence characteristics. The decatungstate anion $[W_{10}O_{32}]^{4-}$, the paratungstate anion $[H_2W_{12}O_{42}]^{10-}$ and the metatungstate anion $[H_2W_{12}O_{40}]^{6-}$ (the latter may also be described in the literature as the dodecatungstate[5], dihydrogendodecatungstate[8] or metadodecatungstate[8] anion) are examples of these arrangements. The two protons of the $[H_2W_{12}O_{40}]^{6-}$ anion are located within the central cavity of the Keggin-like structure and are relatively inaccessible.[8, 9] Due to their rich suite of redox,[10] structural[11] and photo-electronic[12] characteristics, POM-based materials have received attention[13] for applications such as opto-electronic devices,[14] oxidation catalysts,[15] medicine,[16] chemical sensors[17] and mesoporous cationic conductors.[18]

POMs can react with organic cations to form a wide range of hybrid organic-inorganic entities.[4, 11, 13, 19, 20, 21] Within this class of materials, surfactant-POM compounds may be produced by an easily accessible synthesis method that takes advantage of self-assembly techniques.[4, 19, 21] Research within this field greatly benefits from the high manipulability of the self-assembly dynamics where resultant crystallographic structures and other physical properties are dependent upon solution POM concentration and anionic charge, surfactant concentration and cationic charge, surfactant chain length/number, solution pH and temperature. This enables predictable and highly functionalized materials to be achieved.[4, 19, 22] In particular, cationic surfactants can be combined with hydrophilic POMs to generate compounds with layered structures in the solid state.[23] These structures can be readily manipulated as the pore/lamellar sizes are largely dependent on surfactant chain length,[2] pH, POM anionic charge and the resulting surfactant concentration/association.

Thermal treatment may be applied to such a hybrid to remove the more labile organic surfactants, leaving behind a robust inter-connected mesoporous inorganic back-bone.[24] Such porous, interconnected inorganic materials find applications as solid-state cationically-conductive (H^+, Li^+, Na^+, K^+, Rb^+ and Cs^+) devices[25] or catalytic molecular-sieves[24] due to the transition-metal-oxide's desirable electronic structure and physical robustness.[26] Throughout the treatment process, parameters such as physical and electronic structure,[27] expansion/porosity,[28] hydration,[29] stoichiometry and chemical bonding[30] must be known in order to predict the thermally-dependent surfactant-cation/POM-anion dynamics. Stability and quality of the end products is highly dependent on hybrid-framework properties such as counter-cation/surfactant concentration,[18] structure/phase (including pore-size) of the inorganic (POM)[31] and hydration (of the surfactant and the POM), all of which are heavily dependent on the heating parameters. For example, knowing the temperature at which organic surfactants desorb from these materials is necessary to

[a] Institute for Nanoscale Technology, University of Technology Sydney, PO Box 123, Broadway NSW 2007, Australia

†Electronic Supplementary Information (ESI) available: XRD data, TGA data, FTIR and Raman spectra, EDS and XPS spectra. See DOI: 10.1039/x0xx00000x

predict when the sample becomes porous, though it is also necessary to understand the thermal dynamics of the inorganic component to ensure that it does not crystallize into a less-porous bulk oxide phase. The atmosphere of the heating environment also plays a role in processing, with reductive and, to a lesser extent, inert, atmospheres such as H_2 and N_2, accelerating decomposition and driving oxygen-vacancy generation (sub-stoichiometry) at elevated temperatures,[32] as opposed to oxidizing atmospheres, such as air, maintaining stoichiometry though mutually acting as a more aggressive environment towards any organic constituents.

Production of surfactant-POM compounds however, usually involve the mixing of the pre-fabricated aqueous POM and hydrophobic surfactant in multi-pot processes. One-pot synthesis methods provide an attractive cheaper, and more efficient prospect for the production of surfactant-POM compounds and precursors. Here we investigate the one-pot synthesis and thermal decomposition of $(CTA)_6[H_2W_{12}O_{40}].2H_2O$, where CTA^+ = cetyltrimethylammonium cation. We will show that this compound generally contains an additional intercalated (CTA)Cl so, strictly speaking, the formula is $(CTA)_7[H_2W_{12}O_{40}]Cl.2H_2O$. In the discussion that follows we will refer to $(CTA)_7[H_2W_{12}O_{40}]Cl.2H_2O$ as CTA-W_{12}. The behaviour of CTA-W_{12} under both inert (N_2) and oxidizing (air) atmospheres is assessed using thermal gravimetric analysis, differential scanning calorimetric (TGA-SDT), Fourier-transform infra-red spectroscopy (FT-IR) and *in-situ* synchrotron x-ray diffraction (XRD) in order to characterize the structural and chemical transitions that occur upon heating.

Experimental Section

Synthesis of CTA-W_{12}

Cetyltrimethylammonium bromide (0.62 g, 1.72 mmol) was dissolved in de-ionized water (200 mL) at 70°C whilst stirring. Tungsten hexachloride (3.05 g, 7.70 mmol) was then added and the resultant black mixture was allowed to cool to room temperature and stirred for a further 16 h. Aqueous ammonium hydroxide (4.5 mL at 30 wt.% NH_3) was then added to achieve a pH of 7.5 whereupon the color of the mixture changed from yellow to white. The mixture was stirred for 16 h at room temperature and then the solid was collected by filtration and washed five times with de-ionized water. The collected material was dried in air for 72 hrs. Yield of CTA-W_{12} was 0.97 g (80%). Anal. Calcd for $C_{133}H_{300}N_7ClO_{42}W_{12}$: C 32.52, H 6.16, N 2.00. Found: C 32.22, H 6.24, N 2.03. FT-IR: 783, 887, 954, 1376, 1406, 1467, 1488, 1637, 2850, 2918, 2955, 3041, 3141, 3399 cm^{-1}.

X-ray Diffraction

X-ray diffraction (XRD) was carried out at the Australian Synchrotron on the Powder Diffraction beam-line utilizing a photon energy of 18 keV (λ = 0.6887 Å, refined against a LaB_6 standard). Samples were mounted in 0.3 mm diameter SiO_2 capillaries and patterns collected at a rate of one scan per two minutes. Heating of the samples up to 900°C was performed using a Eurotherm hot air-blower. Rietveld refinement of the XRD data was performed in two steps. First, following the example of Stein *et al*,[33] a trial structure of P1 space group in which each Keggin ion was replaced a single heavy metal atom (Au) was fitted to the experimental pattern in a first pass. Next, the Au atoms were replaced by $H_2W_{12}O_{40}$ Keggin ions and the refinement repeated in a second pass. The presence or absence of the surfactant molecules made no difference to the refinement as their contribution is overwhelmed by that of the W atoms.[5] The effect of various orientations of the Keggin ions in space was investigated in a third pass but the only definitive conclusion that could be drawn was that adjacent Keggin ions in the unit cells were oriented differently. Crystal structures were visualized with the VESTA program.[34]

Transmission Electron Microscopy

Transmission electron microscope (TEM) images were collected on a JEM-2200FS Field Emission Microscope. FT-IR spectra were collected on an Agilent ATR FT-IR. Microanalysis for C, H and N was carried out by the University of Otago, New Zealand. XPS measurements were made with a Thermo Scientific® ESCALAB250Xi, utilizing mono-chromated Al K-α (1486.68 keV) radiation at 120 W. The spectrometer was calibrated using Au_{4f7}, Ag_{3d5} and Cu_{2p3} lines at 83.96, 368.21 and 932.62 eV respectively, at a C_{1s} binding-energy reference (284.8 eV for adventitious hydrocarbon).

Other Analyses

TGA/DSC was performed using a SDT Q600® V20.9 operating from 30°C to 950°C at a heating rate of 5°C min^{-1}, utilizing a nitrogen or air gas flow at 100 mL/min. Scanning electron microscope (SEM) images were collected on a Zeiss Supra 55VP SEM, with samples deposited onto a Si wafer with the aid of methanol and left to dry for 24 h.

Results and Discussion

Synthesis of CTA-W_{12}

Tungstates are known to condense by the process of olation into various polyoxoanion clusters in aqueous solution, dependent on solution pH, and concentration and type of ions present.[5, 22, 35, 36] Scheme 1 shows the synthesis of CTA-W_{12} from WCl_6 and CTA-Br in water. Upon mixing WCl_6 with water and CTA-Br, $[CTA]_{(y-x)}[H_xWO_3(OH)_y]$ was formed and was characterized by powder XRD, Raman spectroscopy and FT-IR (Supporting Information, Figure S1. Subsequent addition of ammonium hydroxide to raise the pH to 7.5 gave CTA-W_{12} as a white powder in good yield. Characterization data for CTA-W_{12} are discussed in detail below.

$$WCl_{6(s)} + CTA - Br_{(aq)} \xrightarrow{16hrs} (CTA)_{(y-x)}[H_xWO_3(OH)_y] \xrightarrow{NH_4OH} (CTA)_7[H_2W_{12}O_{40}]Cl \cdot 2H_2O \quad \text{(Scheme 1)}$$

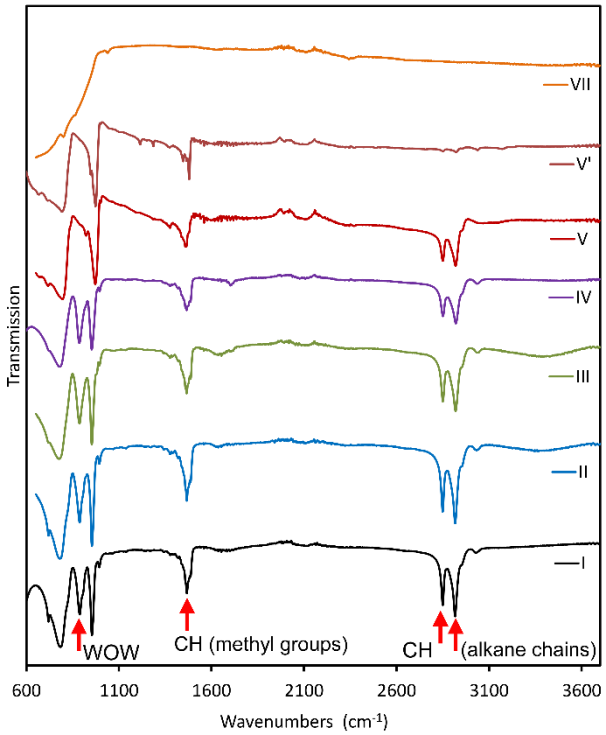

Fig. 1 ATR FT-IR spectra of CTA-W_{12} (I) and the products formed when it is thermally decomposed (II to VII). The features associated with the (-W-O_b-W-) bonds of the Keggin ion, the -CH_3 symmetric bending and 'umbrella vibration' of methyl ammonium groups, and the -CH_2 stretching of the alkane/alkene chains are highlighted. Trace V′ is for phase V after washing in chloroform.

The order of addition of ammonium hydroxide is important; CTA-W_{12} formed only when NH_4OH was added *after* WCl_6 was mixed with water and CTA-Br. Keggin anions are known to form from tungstate solutions in the presence of large quaternary-ammonium cations, at room temperatures and at higher pH.[37, 38] It is thought that these larger cations do not allow the condensation of typical monoclinic, pyrochlore or hexagonal extended structures resultant from precipitation of WO_4^{2-} solutions, but instead favor the formation of larger, higher nuclearity polytungstates[37]

The addition of WCl_6 to pure water at a concentration of 60 g/L in the absence of CTA-Br (Scheme 2) unsurprisingly gave $WO_3.xH_2O$[39] (see Supporting Information, Figure S2 for XRD, Raman and FT-IR data) and a resultant solution pH of ~0.5. After the reaction mixture was aged for 1 day at low pH, addition of CTA-Br yielded a product consisting of lamellar-separated $WO_3.xH_2O$ (by XRD, FT-IR and Raman measurements, Supporting Information, Figure S3) where CTA^+ cations separate the layers of WO_3. Importantly, adding CTA to a mixture of $WO_3.xH_2O$ and then increasing the pH (up to pH 8) of this suspension does not yield CTA-W_{12} (even after 1 week) but rather a variety of isopolytungstates (Supporting Information, Figure S4). Similarly, when a solution obtained from the addition of ammonium hydroxide to $[CTA]_{(y-x)}[H_xWO_3(OH)_y]$ (at pH 8) was acidified with hydrochloric acid (to pH 4), CTA-W_{12} was not obtained, instead various isopolytungstates were produced (Supporting Information, Figure S5).

At moderate temperatures and at higher pH (~8 to 14), tungsten oxides exist as the singly protonated or diprotonated mono-nuclear hydrogen tungstate, $H[WO_4]^-$ or $H_2[WO_4]$, while at low pH (<1) the most stable form is the hydrated bulk trioxide, $WO_3.xH_2O$ (where x generally = 0.33, 0.5, 1 or 2).[35] It is between these extremes that tungsten oxoanions can self-associate to take many forms, including the present metatungstate, $[H_2W_{12}O_{40}]^{6-}$, anion. Here we have shown that the metatungstate CTA-W_{12} is accessible only when the trioxide is formed *in the presence* of CTA-Br and *then* the pH is increased to 7.5. Ban *et al* observed a similar pH-dependent formation of organic-cation:Keggin compounds from tungstate solutions in their study of $(TMA)_6[H_2W_{12}O_{40}].9H_2O$ (where TMA = trimethyl ammonium cation). We propose that at higher pH, the protons within $H_xWO_4^{2-x}$ anions are readily substituted by the larger CTA^+ cations, whereas at lower pH this process is hindered by the formation of $WO_3.xH_2O$ and other isopolyanions. Furthermore, reaction of ammonium metatungstate $(NH_4)_6[H_2W_{12}O_{40}]$ with CTA-Br by cation exchange in water did not produce CTA-W_{12}.

Characterization of CTA-W_{12}

The FT-IR spectrum of CTA-W_{12} (Figure 1) contains bands characteristic of Keggin anions.[6, 33, 40] Considering the bond lengths reported by Asami et al.[8], the band at 783 cm^{-1} can be assigned to ν(-W-O_c-W-) and the 887 cm^{-1} band to ν(-W-O_b-W-) (see Figure S6 for site labelling scheme) while a band at 954 cm^{-1} is assigned to ν(-W=O_d).[33, 41] Aliphatic CTA^+ vibrations appear at 1376, 1406, 1467, 1488, 2850, 2920, 2953 and 3039 cm^{-1} and correspond to ω(-CH_2-) wagging, σ(-CH_3-) 'umbrella' vibration, δ(-CH_2-) scissoring, σ_s(-N^+(-CH_3)) symmetric bending of -CH_3, ν_{ss}(-CH_2-) symmetric stretching, ν_{as}(-CH_2-) antisymmetric stretching, ν_{as}(CH_3-) asymmetric stretching and ν_{as}(-N^+-CH_3) asymmetric stretching of the -CH_3, respectively.[2, 42, 43] Peaks assigned to intercalated H_2O appear at 1637, 3141 and 3399 cm^{-1}. The Raman spectrum of CTA-W_{12} (Supporting Information, Figure S7) also contains bands assigned to the CTA^+ cation as well as a strong ν(W=O) band at 982 cm^{-1}.[44]

XPS data reveal that the tungsten centers are predominantly in the W(VI) oxidation state with a small amount of W(V) present (Figure S8). The latter is due to oxygen-vacancies created during the measurement within the very high-vacuum environment.[45] The spectrum contains signals characteristic of the Keggin cage (-W-O-), a small amount of absorbed moisture (-W-OH), bands assigned to carbon atoms within the alkyl chain and CTA^+ head-group (-C-N-), and a single N band assigned to the nitrogen of the CTA^+ head-group.

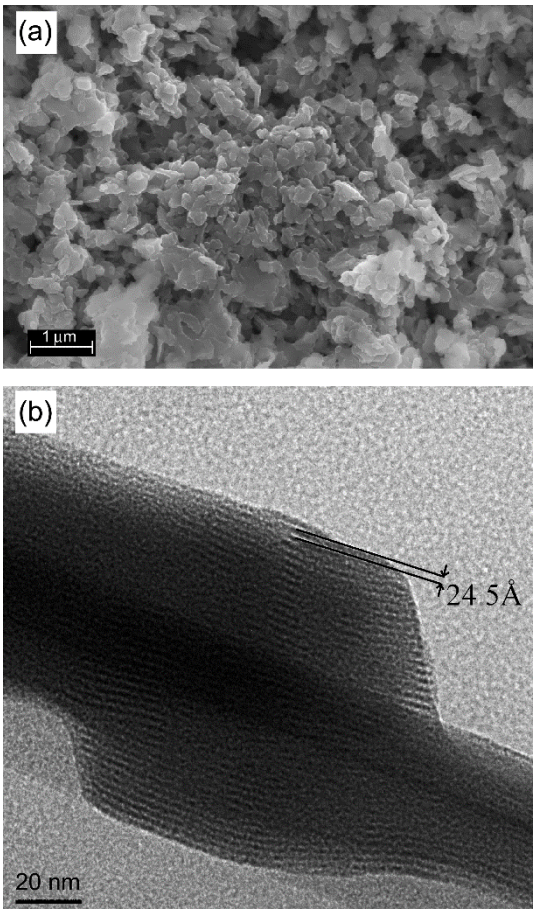

Fig. 2 SEM (a) and TEM (b) images of CTA-W_{12}

Microanalytical data provides a formula of $(CTA)_7[H_2W_{12}O_{40}]Cl.2H_2O$. Using this data, the $W_{12}O_{36}$ component is 56.6% of the mass. Thermogravimetric analysis (discussed in detail below) shows that after calcination to elevated temperatures, the refractory, inorganic portion ($W_{12}O_{36}$ or WO_3) of CTA-W_{12} was 53.9% of the initial mass, consistent with the microanalytical data. The presence of Cl is confirmed by EDX analysis (Supporting Information, Figure S9), however quantitative results from the analysis are not useful due to the inability to analyze for H. Figure 2(a) shows an SEM image of CTA-W_{12} where ~200 nm diameter particles are prevalent. The TEM image is shown in Figure 2

Figure 2(b) reveals planes ~24.5 Å apart (with a spread of 19 Å to 25 Å measured at various positions). Only a single tilt direction provided structural information on any of the particles, a result of the layered structure of surfactant-POM compounds[5] which is prominent when imaged side-on. The sheets are likely to be turbostratic in nature.

The powder XRD pattern (Figure 3) exhibits a peak at low 2θ which corresponds to an interlayer spacing of 24.5 Å, consistent with the TEM data. Similarly, Nyman *et al*[1] and Asami *et al*[8] report inter-layer spacings of 24.44 and 21.46 Å, respectively, for the related compounds $[H_xSiMo_{12}O_{40}][C_{16}H_{33}N(CH_3)_3]_5[CH_3CN]_4$ and $[(CH_3)_4N]_6[H_2W_{12}O_{40}]$.$9H_20$. The length of CTA^+ is ~20.1 Å [46] and so, in the present instance, the cations must be interdigitated to fit between the sheets of $[H_2W_{12}O_{40}]^{6-}$ anions and thus CTA-

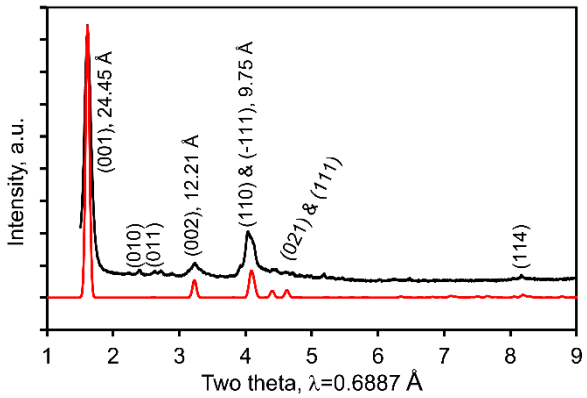

Fig. 3 X-ray diffraction pattern of CTA-W_{12} showing both experimental and fitted pattern. An approximate atomic model of the structure of CTA-W_{12}.

W_{12} falls into the category of 'hyper-digitized' surfactant-POM compounds.[1, 47] Crowding within the hydrophobic interspace results in disordered pseudo-hexagonal arrangements of the templating POM species[47] with the surfactant alkyl-chains tilted off-axis relative to the interface.[47] The irregularity in packing leads to a spread of distances between anions.[1, 47] Chemically similar compounds with lamellar structures and interlayer spacings of 35 to 40 Å have been previously prepared using reaction temperatures between 90 and 170°C.[48,33] Higher reaction temperatures lead to larger lamellar spacings[49] but, as we will show, expansion of the layered structure in CTA-W_{12} can also be induced by raising the temperature of the product synthesized at room temperature. A unit cell with two Keggin ions, oriented similarly, was fitted to the as-synthesized material. Some rotation or loss of symmetry between individual Keggin ions was required to fit the small (010) peak at d= 16.3 Å, which would be absent with a uniform Keggin ion distribution. Similarly, the (101) peak at 10.09 Å can only be generated when one of the Keggin ions in the unit cell is slightly out-of-plane, with z = 0.17. The unit cell parameters were a=12.40±0.10 Å, b= 16.45 ±0.10 Å, c= 24.90±0.20 Å, α= 90°, β= 101.5±0.5° and γ= 90°.

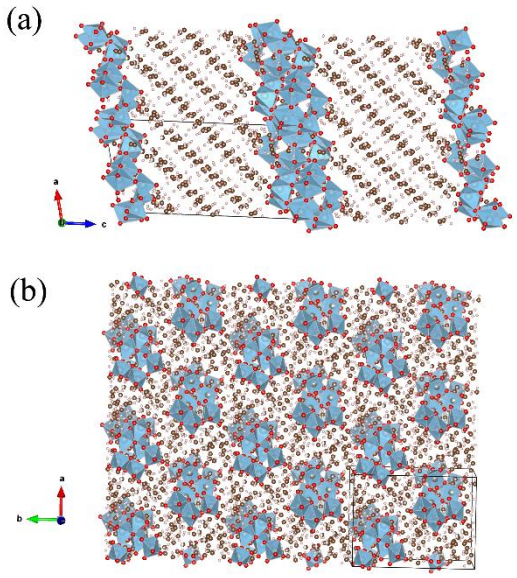

Fig. 4 An approximate atomic model of the structure of CTA-W_{12}. (a) side view showing planes of Keggin ions, (b) top view, showing hexagonal arrangement of Keggin ions. (The carbons and hydrogens shown are only schematic as their positions were not refined due to the dominating effect of the heavy W atoms. Therefore, for these elements, we have used the positions provided by Nyman *et al*[1] for the related compound $[CH_3CN]_2[CTA]_4.[H_2SiMo_{12}O_{40}]$).

The resulting structure, which can be described as consisting of hexagonally packed sheets of Keggin ions separated by a gallery containing the cetyltrimethylammonium ions, is shown in Figure 4. The rotational freedom of the Keggin ions indicates that this material can be considered a metallotropic, smectic liquid crystal.[48, 49] The pseudo-hexagonal packing of the $[H_2W_{12}O_{40}]^{6-}$ anions is evidenced by the asymmetric peak at d= 9.8 Å (Figure 3).

Thermal decomposition of CTA-W_{12}

DTA/TGA data revealed that the decomposition of CTA-W_{12} in air proceeded between 210 and 500 °C in three distinct stages of mass loss, accompanied by two endothermic events and three major exothermic events, Figure 5. In contrast, mass loss in a nitrogen atmosphere also began at 210°C but was completed by 389°C. A sequence of X-ray diffraction patterns collected at increasing temperature using synchrotron radiation is shown in Figure 6. There are at least seven distinct phase transitions. To simplify the discussion we have labelled the phases involved as I - VIII, where phase I is the CTA-W_{12} discussed above. No matches could be found for phases I to V in the JC-PDF or COD databases. *Ex situ* FT-IR spectra, Figure 1, was recorded to investigate the chemical changes that accompanied the thermal transitions and structural changes of CTA-W_{12} when heated in air. The data from the DTA, TGA, XRD and FT-IR can be examined collectively to produce a complete description of the thermal decomposition of CTA-W_{12}.

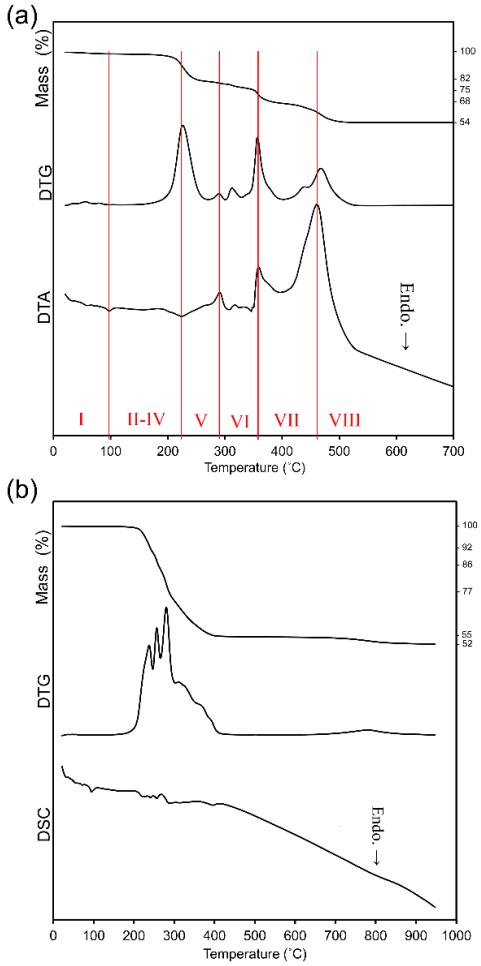

Fig. 5 TGA-SDT curve of CTA-W_{12} at 5°C/min, (a) in air, (b) in nitrogen. The approximate ranges of stability of structures I to VIII are shown in (a).

Phase I (CTA-W_{12}) lost mass at ~60°C when heated in air, which we assign to loss of two molecules of H_2O. This phase was otherwise stable up to ~80°C (synchrotron data) or 98°C (DTA). At 98°C, an endothermic event was observed in the TGA (with no associated mass loss) and an increase in the intensity of the (002) lamellar-spacing peak, Figure 7, indicating the onset of phase II. A shift towards lower 2θ was observed indicating an increase in the inter-layer distance arising due to the tilted CTA^+ chains adopting a more normal orientation relative to the hydrophobic/hydrophilic interface.[50] The inter-layer distance increased monotonically until 185°C. Phase III is defined by the emergence of two new diffraction peaks at d= 17.00 and 14.86 Å, which persist until 222°C. The (001) lamellar spacing (calculated from the (002) data) was 28 to 31 Å, a distance for which the CTA-tails must still be interdigitated. None of the phases I-III displayed an XRD pattern matching that of the $(CTA)_6W_{12}$ compound synthesized by Stein *et al*[33] by prolonged hydrothermal treatment at 100 to 150°C (but measured at room temperature). This suggests that at least four different metallotropic structures are possible in

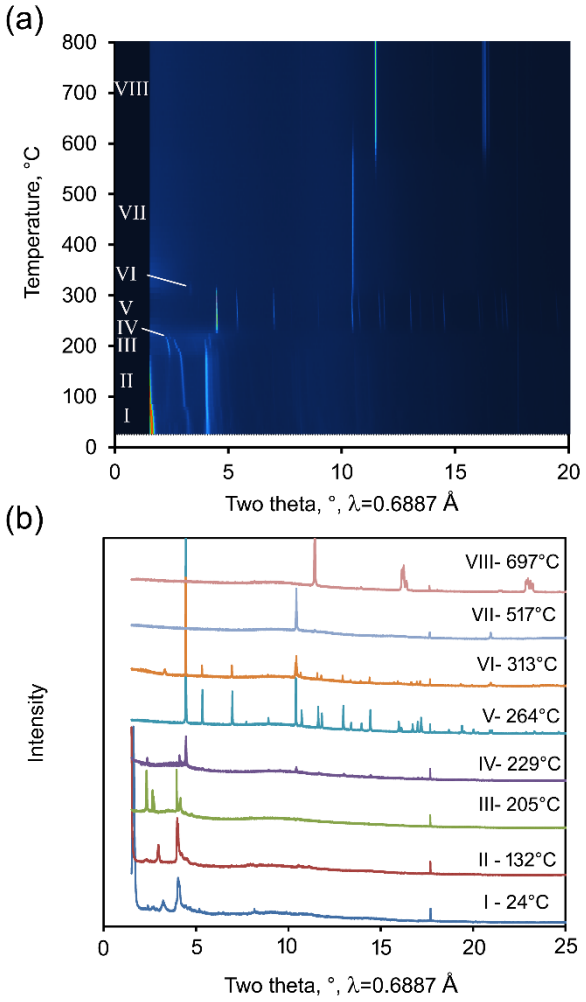

Fig. 6 Synchrotron XRD patterns of CTA-W_{12} undergoing thermal decomposition when heated at 5˚C/min in air, obtained with λ = 0.6887 Å, (a) iso-intensity map of diffraction patterns, (b) characteristic diffraction patterns of different structures.

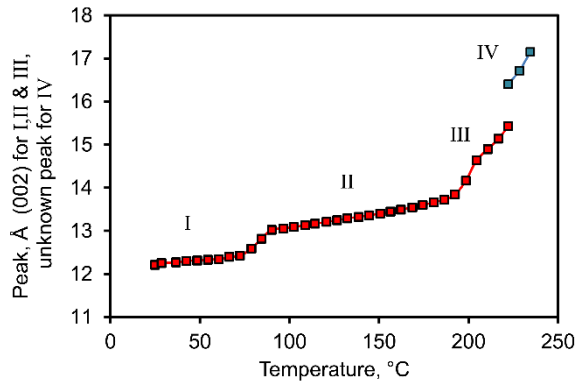

Fig. 7 Expansion of (002) plane between room temperature and 217°C. Phases I, II and III share a continuous (002) reflection but there is a first-order transition from III to IV.

this system with the outcome of the synthesis depending on temperature and synthesis conditions.

The location of the ν_{ss}(-CH_2) and ν_{as}(-CH_2-) bands, 2850 cm^{-1} and 2918 cm^{-1}, respectively, in the FT-IR spectrum indicates that the alkyl chains are not bent.[43, 50, 51] Thus, the changes in inter-layer distances from I to II to III are assigned to tilting and/or relaxation of the interdigitation and not an increase in gauche-related disorder.[50] In addition, the continuity of the X-ray diffraction patterns suggest that I→II and II→III were second-order transitions, *i.e.* the structure of each low temperature phase morphed smoothly into that of the higher temperature phase without nucleation and growth of new crystals.

There was significant mass loss from 210°C onwards associated with an endothermic process in both air and N_2 environments, coincident with the decomposition of phase III.

It is instructive to briefly discuss the decomposition of CTA-Br (Figure S10), both as a pure substance and as an occlusion within a porous oxide matrix so that this behavior can be compared to that of the present samples. In the case of pure CTA-Br, decomposition in air occurs in a single, endothermic step between 230 and 250°C[52] with emission of some gases. In contrast, when CTA-Br is within a porous SiO_2 matrix, decomposition in air proceeds in three steps: first a mass loss of ~50% between about 150 and 250°C, and then a mass loss of ~20 % between about 250 and 300°C, with the final fraction of the organics surviving up to 500 to 600°C as a soft coke.[52, 53] The nature of the oxide is important: in titania-based materials, decomposition of the CTA-Br takes place in a single oxidative step at ~300°C with simultaneous emission of alkyl fragments.[52] In silica, the initial decomposition of the CTA-Br proceeds by cleavage of the head group to give trimethylamine (b.p.=5°C and hence rapidly volatilized) at 150 to 250°C, while the tail becomes hexadecene (b.p.=274°C), which is retained in the sample to its boiling point and presumably partially converted to soft coke.[52] A change in the ambient environment is significant: Goworek *et al*[54] reported that CTA-Br/SiO_2 decomposed under hydrogen to a mixture containing trimethylamine, 1-hexadecene and N,N-dimethylhexadecylamine (b.p.=150°C) at temperatures as low as 150°C.[54] At 300°C the formation of N,N,N-trihexadecylamine was reported. Presumably, any of these hexadecylamines boil off as soon as they are formed.

In our sample the loss of mass from the CTA-W_{12} proceeded step-wise in air through to 500°C accompanied by exothermic combustion peaks at 290, 360 and 460°C, in contrast to inert N_2 where mass loss was complete by 390°C and endothermic in nature. Considering the endothermic event between 210 and 250°C, we propose that the CTA^+ cracked at these temperatures, producing a mix of trimethyl-ammonium ($(CH_3)_3NH^+$), 1-hexadecene ($(CH_3)(CH_2)_{13}CH=CH_2$), N,N-dimethyl-hexadecylamine ($(CH_3)(CH_2)_{15}N(CH_3)_2$) and $CH_3^{\bullet}$ (which would react with H_2O or H^+ to produce volatile CH_4 or CH_3OH) together with H_2O.[54] Then, partial oxidation of these CTA^+ decomposition products occurred at 360°C to give a residue (similar to the 'soft coke' reported by Kleitz[52]) that combusted at 460°C. Coincident with these chemical changes, XRD data showed that between 222 and 235°C, a completely different structure formed, designated here as IV. The discontinuity in the X-ray diffraction patterns strongly suggests that III→IV was a first-order transition, *i.e.* crystals of IV nucleated and grew out of a matrix of III. FT-IR spectra indicated that phase IV contained Keggin ions and some alkane and quaternary-amine groups.

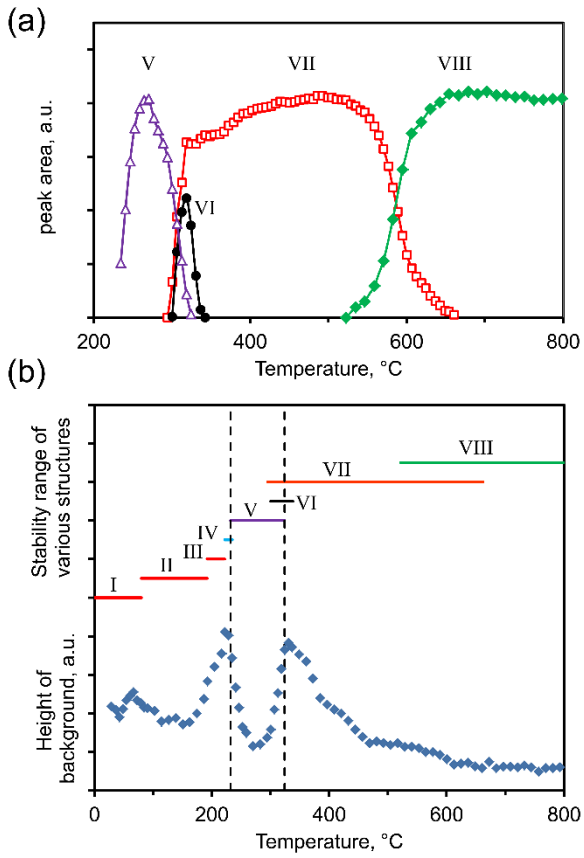

Fig. 8 Conversion of phase V to VI to VII to VIII during heating ramp,(a) followed using the area under a characteristic peak for each phase (phase V- peak at *d*=8.87 Å , phase VI- peak at *d*=11.94 Å, phase VII- peak at *d*=3.79Å, phase VIII- peak at *d*=3.46Å), (b) increase in amorphous background (represented by intensity of pattern at *d*=19.7 Å) with stability ranges of various phases superimposed. Note that the highly crystalline phase V forms from a relatively disordered precursor, and then decomposes to produce an initially relatively disordered product.

At 235°C, phase IV disappeared in another first-order transition and was replaced by phase V, which was characterized by a very well-formed series of diffraction peaks spread across 2θ. Phase V was stable between 235 and 310°C. A further exothermic mass loss of about 8% occurred between 250 and 350°C, most likely attributable to combustion of 1-hexadecene and N,N-dimethylhexadecylamine (b.p. 274 and 324°C, respectively). Correspondingly, FT-IR bands assigned to organic components (>1300 cm^{-1}) decreased in intensity. Also within this temperature range, the ν(-W-O_b-W-) peak at 887 cm^{-1} disappeared, the ν(-W-O_c-W-) blue-shifts to 796 cm^{-1}, and the ν(-W=O_d) peak also blue-shifts and splits to form maxima at 923 and 973 cm^{-1}. This latter change probably marks the decomposition of the Keggin-anion to lower-nuclearity structures, most likely hepta- and octa-tungstate-like compounds.[55, 56] Similar changes in vibrational spectra have been reported for the conversion of ammonium metatungstate to WO_3[6] and the thermal decomposition of the Keggin salt $H_4PVMo_{11}O_{40}$[55] and $H_3PMo_{12}O_{40}{\cdot}30H_2O$.[56] Computational studies of other, related, Keggin heteropolyacids have reported that the O_b bond would be the first to be eliminated during thermal decomposition.[57] Alkyl-chain (1-hexadecene and N,N-dimethylhexadecylamine) and ammonium species are still present at 250°C, as confirmed by FT-IR (Figure 1, V). To remove these lipophilic components from this phase, a Soxhlet extraction with chloroform ($CHCl_3$) was applied for over 12 hours to remove any soluble products. The absence of δ(-CH_2-), ν_{ss}(-CH_2-), ν_{as}(-CH_2-) (1464, 2850 and 2920 cm^{-1}, respectively) within the FT-IR spectrum of the washed compound confirmed the removal of alkane species (phase V′, Figure 1). Microanalysis of this phase produced values of 23.93 % C, 1.41% N and 3.34% H before washing, and 14.84% C, 1.68% N and 2.26% H after washing. The absence of alkane peaks, the increase in the intensity of the ν_{as}(N-R_4^+) band (at 3039 cm^{-1}), and the increase in the N:H ratio after washing in $CHCl_3$ (0.42 and 0.74 for un-washed an washed samples, respectively) is evidence that soluble 1-hexadecene and N,N-dimethylhexadecylamine components have been removed, leaving behind insoluble cationic compounds, notably $(CH_3)NH^+$, and some soft coke.

Corner-sharing W-O_b-W bonds hold the triads (three octahedra joined together) of the Keggin anion together. The absence of these bonds in phase V suggests that the original Keggin ions have broken apart[55] when phase V formed. Since phase V is not yet a bulk oxide, due to the presence of the strong ν(-W=O_d) vibration,[58] it follows that the remains of the Keggin ions must have reorganized into some other form. One likely possibility is that the anion has reorganized into heptatungstate fragments (or possibly the similar octatungstate), analogous to the case for Mo POM hexakis (*tert*-butylammonium) heptamolybdate.[59] Considering the FT-IR, TGA and microanalysis data, it is possible that phase V is a heptatungstate ($[W_7O_{24}]^{7-}$) with an average of 2.5 trimethylammonium and 4.5 acidic hydrogen cations ($(((CH_3)NH)_{2.5}.H_{4.5}[W_7O_{24}]$). The presence of the acidic hydrogens is indicated by the broad ν(-OH) and δ(-OH) deformation bands in the FT-IR around 1600 and 3400 cm^{-1}. Support for the existence of these acidic hydrogens in phase V can be found in the literature[58] where it is stated that protons most likely associate with the closely related molybdate fragments mentioned above up until 520°C, just prior to the emergence of the bulk oxide. Indeed it is stated by Mestl *et al*[55] that in order for fragments to condense into the bulk trioxide, complete dehydration of the fragments must take place. It is also found that heating rates above 0.2°C/min are too fast for water to be completely evacuated from the compound prior to Keggin fragmentation, and faster heating rates (such as the 6°C/min used here) will affect decomposition kinetics. It is therefore feasible that acidic hydrogens are present within the compound up until the emergence of the bulk oxide (at 350°C), in accordance with previous studies.

A unit cell with *a*=8.493 Å, *b*=8.493 Å, *c*=8.861Å, α = β = 90°, γ =120° was suggested for phase V by analysis of the X-ray diffraction pattern. This is too small to contain a complete Keggin ion: for example, in body-centered cubic anhydrous ammonium metatungstate, the meta-crystal unit cell has a volume[5] of 927 $Å^3$ per Keggin ion whereas the present unit cell only has a volume of 544 $Å^3$. However, the present unit cell is a good match for a single heptatungstate moiety, or, if the c-axis is doubled in length, for two such entities (Suppoeting Information, Figure S11). A calculated density of the order of 5.0 to 5.1 g/cm^3 would result. This is reasonable as bulk WO_3 has a density of about 7 g/cm^3. We propose that the structure of phase V is a simple hexagonal crystal, in which some presently unknown fragment of the Keggin ions form the principal diffracting units.

Figure 8 displays selected X-ray data spanning the transformation of phases V, VI, VII and VIII. The transformations

from IV →V, V→VI and/or V→ VII are complex, Figure 8(a). There is an increase in the amorphous component of the material upon proceeding from IV→V and as phase V decomposes, Figure 8(b). The decomposition of V was marked by the appearance of phase VI, which existed in a narrow temperature range of 300 - 335°C. The XRD diffraction pattern of VI differed from that of phase VII only by the appearance of a strong peak at d = 11.93 Å. The area of the representative XRD peak chosen for phase V reduced sharply at 265°C but the areas of the peaks chosen for VI and VII started to increase only at 300°C. There was, however, no other crystalline phase in the range 265 - 300°C that increased at the expense of the decomposition of V. Therefore, there must be significant amorphization of the sample and of compound V, within this range of temperature. At 300°C phases VI and VII nucleate and there was a sharp increase in their volume fractions and an associated 7% mass loss. Loss of any constitutional H^+ within the Keggin fragments (as water) could be responsible for part of this mass loss as that is a necessary step in the conversion to the bulk oxide.[57] There was a slow increase in the peak area for VII between 320 and 490 °C. There is a relatively large exothermic event at ~470°C (when heated in air) and a further 12% mass loss with little mass lost above that temperature. It is likely that this exothermic peak is mostly due to oxidation of the carbonaceous 'soft coke' although some contribution from the crystallization of the bulk oxide[57] cannot be ruled out. The increase in the height of the XRD peaks for VII indicates an increase in the amount of this phase within the sample. Clearly, in this range of temperatures, phase VII is crystallizing from the amorphous material rather than directly from phase V or VI since these have already disappeared by these temperatures. Further work to elucidate the mechanism of this transition would be of interest.

The diffraction pattern of VII could be matched with $W_{17}O_{47}$ (COD entry 96-210-7066) while that of VIII matched WO_2 (JC-PDF 01-086-0134), Interestingly, samples heated to 550°C in a laboratory muffle furnace in air converted to yellow monoclinic WO_3 (JC-PDF 01-089-4476) whereas a sample heated to 800°C in a stream of N_2 in a TGA instrument consisted of an 89:11 mixture of WO_3:WO_2 (as determined by Rietveld refinement). The environment within the silica capillary of the synchrotron experiment would be more reducing at elevated temperatures (due to the presence of pyrolysis products of the CTA^+) than the stream of inert N_2 gas was in the TGA instrument, and of course both are less oxidizing than laboratory air.

The synchrotron study showed that the $W_{17}O_{47}$ phase (VII) transformed into black monoclinic WO_2 (JC-PDF 01-086-0134) between 530 and 640°C, with the two phases coexisting over that temperature range. Above 640°C, and up to 800°C, the synchrotron sample consisted only of the black monoclinic WO_2 (JC-PDF 01-086-0134). The transition from phase VII to phase VIII is classic first-order, with phase VII disappearing as phase VIII grows, and the two phases co-existing between 535 and 650°C.

As noted previously, somewhat different results were obtained when calcination was conducted under nitrogen. In general, the endpoint of the thermal transitions of CTA-W_{12} in N_2, as seen in Figure 5, are accelerated relative to those in air. Across the decomposition profile, CTA-W_{12} undergoes three major, narrowly separated mass loss events under nitrogen, without any significant heat exchanges with the environment. The first major mass loss event begins at ~210°C with the release of CTA^+ and dehydration, coinciding with a small endothermic signal. This is closely followed at 240˚C with a similar event (release of organic CTA^+), in the range 260 to 280°C. Decomposition and associated mass loss continues from 300°C to ~410°C, although at a much more steady rate as compared to mass losses 1,2 and 3 (Figure 5) at lower temperatures, as any remaining organic CTA^+ evacuates the sample. From ~650°C, temperatures are sufficiently elevated to drive oxygen-vacancy generation within the lattice[32] and hence sub-stoichiometry in the inert atmosphere,[60] as is evidenced by the ongoing small mass loss of 3% above 800°C resulting in a sub-stoichiometric oxide of $WO_{2.65}$ at 950°C.

Conclusions

A hybrid surfactant-isopolytungstate compound was synthesized from $[H_2W_{12}O_{40}]^{6-}$ and CTA^+ in an aqueous environment to form a lamellar-structure that we designate as CTA-W_{12}. The synthesis of CTA-W_{12} was found to be highly dependent on solution pH and the timing of surfactant addition.

When heated in air, CTA-W_{12} exhibits a sequence of phase transitions. The first three structures are liquid-crystal-like mesoscale phases, with phase I changing to II at 75°C and phase II changing to III at 193°C. The I→II transition is accompanied by a minor mass losses, due probably only to the elimination of some entrained moisture. However, at 222°C the structure is reformed to a compound of unknown structure which we label as IV. Phase IV then transforms to a phase V at 234°C which is characterized by a well-developed X-ray diffraction pattern. Phase V consists of hexagonally packed sheets of fragments derived from the original Keggin ion. There is still a substantial fraction of organic material present at this stage, some of which turned out to be extractable by Soxhlet extraction with chloroform. Heating in N_2 accelerates decomposition by ~100°C relative to events in air.

At 310°C the phase V is converted to a series of bulk oxides which we labeled as VI, VII and VIII. The stoichiometry of the final product obtained depended on the environment in which calcination was conducted, and varied from WO_3 to WO_2. Some of the organic content persisted within the material until 550°C, presumably as soft coke and then elemental carbon, after which it was finally burnt out.

Acknowledgements

Part of this research was undertaken on the Powder Diffraction beamline at the Australian Synchrotron, Victoria, Australia and we thank beamline scientists Dr Quinfen Gu and Dr J. Kimpton for assistance.

Notes and references

1. M. Nyman, M. Rodriguez, T. Anderson and D. Ingersoll, *Crystal Growth & Design*, 2009, **9**, 3590-3597.
2. B. Ingham, S. Chong and J. Tallon, *J. Phys. Chem. B*, 2005, **109**, 4936-4940.
3. N. N. Greenwood and A. Earnshaw, *Chemistry of the Elements*, 2nd edn., Pergamon Press, Oxford Butterworth-Heinemann, 1997.
4. A. Nisar and X. Wang, *Dalton Trans.*, 2012, **41**, 9832-9845.
5. J. Christian and M. Whittingham, *J. Sol. State Chem.*, 2008, **181**, 1782-1791.
6. D. Hunyadi, I. Sajo and I. Szilágyi, *J. Therm. Anal. Calorim.*, 2014, **116**, 329–337.

7. D.-L. Long, R. Tsunashima and L. Cronin, *Angew. Chem. Int. Ed.*, 2010, **49**, 1736-1758.
8. M. Asami, H. Ichida and Y. Sasaki, *Acta Cryst.*, 1984, **C40**, 35-37.
9. C. Sprangers, J. Marmon and D. Duncan, *Inorg. Chem.*, 2006, **45**, 9628-9630; V. F. Chuvaev, K. I. Lunk, I. D. Kolli and V. I. Spitsyn, *Izvesttiya Akademii Nauk SSR, Seriya Khimicheskaya*, 1969, **2**, 243-246 (in translation).
10. W. Qi, Y. Wang, W. Li and L. Wu, *Chem. Eur. J.*, 2010, **16**, 1068-1078.
11. A. Dolbecq, E. Dumas, C. Mayer and P. Mialane, *Chem. Rev.*, 2010, **110**, 6009-6048.
12. M. Wang, G. Xu, Z. Zhang and G. Guo, *Chem. Commun.*, 2010, **46**, 361-376.
13. A. Proust, B. Matt, R. Villanneau, G. Guillemot, P. Gouzerha and G. Izzet, *Chem. Soc. Rev.*, 2012, **41**, 7605-7622.
14. T. He and J. Yao, *Progr. Mater. Sci.*, 2006, **51**, 810-879.
15. A. Proust, R. Thouvenot and P. Gouzerh, *Chem. Commun.*, 2008, **2008**, 1837-1852.
16. J. Rhule, C. Hill and D. Judd, *Chem. Rev.*, 1998, **98**, 327-357.
17. S. Herrmann, C. Ritchie and C. Streb, *Dalton Trans.*, 2015, **44**, 7092-7104.
18. I. Szilágyi, J. Madarász, G. Pokol, P. Király, G. Tárkányi, S. Saukko, J. Mizsei, A. Toth, A. Szabo and K. Varga-Josepovits, *Chem. Mater.*, 2008, **20**, 4116-4125.
19. P. Yin, D. Li and T. Liu, *Chem. Soc. Rev.*, 2012, **41**, 7368-7383; T. Zhang, J. Brown, R. Oakley and C. Faul, *Current Opinion in Colloid & Interface Science*, 2009, **14**, 62-70.
20. D. Du, J. Qin, S. Li, Z. Su and Y. Lan, *Chem. Soc. Rev.*, 2014, **43**, 4615-4632; D. Long, R. Tsunashima and L. Cronin, *Angew. Chem. Int. Ed.*, 2010, **49**, 1736 – 1758.
21. Y. Yan and L. Wu, *Isr. J. Chem.*, 2011, **51**, 181 – 190.
22. D. Long, E. Burkholder and L. Cronin, *Chem. Soc. Rev.*, 2007, **36**, 105-121.
23. S. Polarz, S. Landsmann and A. Klaiber, *Angew. Chem. Int. Ed.*, 2014, **53**, 946-954.
24. B. Holland, P. Isbester, E. Munson and A. Stein, *Mater. Res. Bull.*, 1999, **34**, 471-482.
25. C. Dey, T. Kundu and R. Banerjee, *Chem. Commun.*, 2012, **48**, 266-268.
26. S. Yoon, C. Jo, S. Y. Noh, C. W. Lee, J. H. Song and J. Lee, *Phys. Chem. Chem. Phys.*, 2011, **13**, 11060–11066.
27. J. Wienold, O. Timpe and T. Ressler, *Chem. Eur. J.*, 2003, **9**, 6007-6017.
28. K. Nowinska, R. Fórmaniak, W. Kaleta and A.Wacław, *Applied Catalysis A: General*, 2003, **256**, 115-123.
29. J. Zhou, P. Yin, X. Chen, L. Hu and T. Liu, *Chem. Commun.*, 2015, **51**, 15982-15985.
30. Z. He, Y. Yan, B. Li, H. Ai, H. Wang, H. Li and L. Wu, *Dalton Trans.*, 2012, **41**, 10043-10051.
31. B. Li, J. Zhang, S. Wang, W. Li and L. Wu, *Eur. J. Inorg. Chem.*, 2013, **2013**, 1869-1875.
32. M. Ramzan and R. Brydson, *Sensors Actuators: A*, 2005, **118**, 322-331.
33. A. Stein, M. Fendorf, T. Jarvie, K. Mueller, A. Benesi and T. Mallouk, *Chem. Mater.*, 1995, **7**, 304-313.
34. K. Momma and F. Izumi, *J. Appl. Cryst.*, 2011, **44**, 1272-1276.
35. J. Cruywagen and I. van der Merwe, *J. Chem. Soc. Dalton Trans.*, 1987, **1987**, 1701-1705; F. Di-Natale and A. Lancia, *Ind. Eng. Chem. Res.*, 2007, **46**, 6777-6782; B. Bilal, P. Haufe and R. Moller, *Physica B+C*, 1986, **139-140**, 721-724; S. Prasad, *Química Nova*, 1994, **17**, 31-34.
36. L. Pettersson, *Molecular Engin.*, 1993, **3**, 29-42; L. Fan, J. Cao and C. Hu, *RSC Adv.*, 2015, **5**, 83377-83382.
37. T. Ban, T. Ito and Y. Ohya, *Inorg. Chem.*, 2013, **52**, 10520−10524; P. Zavalij, J. Guo, M. Whittingham, R. Jacobson, V. Pecharsky, C. Bucher and S. Hwu, *J. Solid State Chem.*, 1996, **123**, 83–92.
38. M. Whittingham, J. Guo, R. Chen, T. Chirayil, G. Janauer and P. Zavalij, *Solid State Ionics*, 1995, **75**, 257-268.
39. H. Choi, Y. Jung and D. Kim, *J. Am. Ceram. Soc.*, 2005, **88**, 1684–1686.
40. G. Janauer, A. Dobley, J. Guo, P. Zavalij and M. Whittingham, *Chem. Mater.*, 1996, **8**, 2096-2101.
41. C. Rocchiccioli-Deltcheff, M. Fournier, R. Franck and R. Thouvenot, *Inorg. Chem.*, 1983, **22**, 207-216; R. Thouvenot, M. Fournier, R. Franck and C. Rocchiccioli-Deltcheff, *Inorg. Chem.*, 1984, **23**, 598-605.
42. N. Venkataraman and S. Vasudevan, *J. Phys. Chem. B*, 2001, **105**, 7639-7650; X. Yu, *Microporous Mesoporous Mater.*, 2007, **98**, 70–79.
43. R. Vaia, R. Teukolsky and E. Giannelis, *Chem. Mater.*, 1994, **6**, 1017-1022.
44. R. Buckley and R. Clark, *Coord. Chem. Rev.*, 1985, **65**, 167-218.
45. F. Jones, R. Dixon and A. Brown, *Surf. Sci.*, 1996, **369**, 343-350; S. Klotsmana, V. Kaigorodova, A. Ermakovb and V. Rudenko, *Mater. Lett.*, 2005, **59**, 166–170.
46. S. Yuan, L. Ma, X. Zhang and L. Zheng, *Colloids and Surfaces A: Physicochem. Eng. Aspects*, 2006, **289**, 1-9.
47. M. Nyman, D. Ingersoll, S. Singh, F. Bonhomme, T. Alam, C. Brinker and M. Rodriguez, *Chem. Mater.*, 2005, **17**, 2885-2895.
48. Q. Huo, D. Margolese, U. Ciesla, D. Demuth, P. Feng, T. Gier, P. Sieger, A. Firouzi, B. Chmelka, F. Schuth and G. Stucky, *Chem. Mater.*, 1994, **6**, 1176-1191.
49. W. Li and L. Wu, *Chin. J. Chem.*, 2015, **33**, 15-23.
50. W. Li, S. Yi, Y. Wu and L. Wu, *J. Phys. Chem. B*, 2006, **110**, 16961-16966.
51. N. Venkataraman and S. Vasudevan, *J. Phys. Chem. B*, 2001, **105**, 7639-7650.
52. F. Kleitz, W. Schmidt and F. Schüth, *Microporous and Mesoporous Materials*, 2001, **44-45**, 95-109.
53. M. T. J. Keene, R. D. M. Gougeon, R. Denoyel, R. K. Harris, J. Rouquerol and P. L. Llewellyn, *J. Mater. Chem.*, 1999, **9**, 2843-2850; D. Stojaković, N. Rajić, M. Mrak and V. Kaučič, *J. Serb. Chem. Soc.*, 2007, **72**, 1309–1319.
54. J. Goworek, A. Kierys, W. Gac, A. Borówka and R. Kusak, *J. Thermal Anal. Calorimetry*, 2009, **96**, 375-382.
55. G. Mestl, T. Ilkenhans, D. Spielbauer, M. Dieterle, O. Timpe, J. Kröhnert, F. Jentoft, H. Knözinger and R. Schlögl, *Applied Catalysis A: General*, 2001, **210**, 13-34.
56. H. Nair, J. Miller, E. Stach and C. Baertsch, *J. Catal.*, 2010, **270**, 40–47.
57. M. J. Janik, B. B. Bardin, R. J. Davis and M. Neurock, *J. Phys. Chem. B*, 2006, **110**, 4170-4178.
58. S. Damyanova and J. Fierro, *Chem. Mater.*, 1998, **10**, 871-879.
59. P. Román, A. S. José, A. Luque and H. M. Gutiérrez-Zorrilla, *Acta Cryst.*, 1994, **C5**, 1031-1034.
60. W. Li, A. Sasaki, H. Oozub, K. Aoki, K. Kakushima, Y. Kataoka, A. Nishiyama, N. Sugii, H. Wakabayashi, K. Tsutsui,

K. Natori and H. Iwai, *Microelectronics Reliability*, 2015, **55**, 407-410.